Alzheimer's disease-like paired helical filament assembly from truncated tau protein is independent of disulphide cross-linking

Article (Published Version)

Alzheimer's Disease-like Paired Helical Filament Assembly from Truncated Tau Protein Is Independent of Disulfide Crosslinking

Youssra K. Al-Hilaly[1,2], Saskia J. Pollack[1], Devkee M. Vadukul[1], Francesca Citossi[1], Janet E. Rickard[3], Michael Simpson[4], John M.D. Storey[4,5], Charles R. Harrington[3,5], Claude M. Wischik[3,5] and Louise C. Serpell[1]

*1 - **Dementia Research group,** School of Life Sciences, University of Sussex, Falmer, E, Sussex BN1 9QG, United Kingdom*
*2 - **College of Sciences,** Chemistry Department, Al-Mustansiriyah University, Baghdad, Iraq*
*3 - **Institute of Medical Sciences,** University of Aberdeen, Aberdeen AB25 2ZP, United Kingdom*
*4 - **Department of Chemistry,** University of Aberdeen, Aberdeen AB24 3UE, United Kingdom*
*5 - **TauRx Therapeutics Ltd.,** Aberdeen, AB25 2ZP, United Kingdom*

***Correspondence to Claude M. Wischik and Louise C. Serpell:** cmw@taurx.com; L.C.Serpell@sussex.ac.uk*
https://doi.org/10.1016/j.jmb.2017.09.007
Edited by Sheena Radford

Abstract

Alzheimer's disease is characterized by the self-assembly of tau and amyloid β proteins into oligomers and fibrils. Tau protein assembles into paired helical filaments (PHFs) that constitute the neurofibrillary tangles observed in neuronal cell bodies in individuals with Alzheimer's disease. The mechanism of initiation of tau assembly into PHFs is not well understood. Here we report that a truncated 95-amino-acid tau fragment (corresponding to residues 297–391 of full-length tau) assembles into PHF-like fibrils *in vitro* without the need for other additives to initiate or template the process. Using electron microscopy, circular dichroism and X-ray fiber diffraction, we have characterized the structure of the fibrils formed from truncated tau for the first time. To explore the contribution of disulfide formation to fibril formation, we have compared the assembly of tau(297–391) under reduced and non-reducing conditions and for truncated tau carrying a C322A substitution. We show that disulfide bond formation inhibits filament assembly and that the C322A variant rapidly forms long and highly ordered PHFs.

Introduction

Alzheimer's disease (AD) is characterized by the intracellular accumulation of insoluble neurofibrillary tangles composed of tau protein and the extracellular deposition of amyloid plaques. Amyloid plaques are composed predominantly of the amyloid β peptide [1], while neurofibrillary tangles are composed of paired helical filaments (PHFs), consisting of a truncated fragment of tau protein restricted to the repeat domain [2]. Tau and amyloid β peptides self-associate *in vitro* to form fibrils that share a cross-β core [3,4]. Oligomeric species of tau have been implicated as being important in the characteristic spread of neurofibrillary degeneration throughout the brain and for the toxic effects leading to neuronal dysfunction and death [5,6]. Several lines of evidence point to the importance of neurofibrillary tau pathology being closely associated with dementia in AD and other tauopathies [7–13].

Tau protein, encoded by the *MAPT* gene, is expressed in the central nervous system as a family of six isoforms. These arise by alternative mRNA splicing and vary in length and in the content of three or four tandem repeats of 31 or 32 amino acids in the C-terminal domain [14]. Microtubules are essential in morphogenesis, cell division, and intracellular trafficking of organelles. At physiological concentrations, tau proteins stabilize microtubules as tracks for intracellular transport, but in excess, they interfere with axonal transport [15]. Tau is also implicated in a number of other cellular functions, such as signal transduction and actin interaction and in the binding of pericentomeric chromatin in the nucleus [16,17]. In AD and other tauopathies, tau self-assembles through the repeat domain to form PHFs and straight filaments

(SFs). Structural characterization of PHFs isolated from AD brain tissue has revealed that the fibers display a distinct organisation of paired filaments that either twist [18] or remain straight [3,19,20]. These filaments are also known to share the structural characteristics for amyloid, such as long unbranching filaments and high β-sheet content, and they display the characteristic cross-β pattern by X-ray fiber and electron diffraction [3].

Several groups have investigated assembly of full-length tau *in vitro* using addition of other polyanionic molecules, such as heparin, RNA, or proteoglycans, to nucleate assembly [21–23]. The tau species making up the proteolytically stable structural core of the PHF and its oligomeric precursors are derived from a mixture of fragments derived from both three- and four-repeat isoforms, but restricted to the equivalent of three repeats in length with distinct species originating from the three- and four-repeat isoforms of tau [24]. Two of the fragments from the three- and four-repeat isoforms terminate at the C-terminus at Glu-391, with an N-terminus at amino acid 297. The third derives from the first three repeats of the four-repeat isoform and has N- and C-termini at homologous positions [24,25]. The fragments terminating at Glu-391 can be detected specifically using the antibody mAb423 [26], which has been shown to bind to intra- and extracellular NFTs in AD brain tissue [25,27,28]. The features of these 95-amino-acid-long fragments represent the footprint of the pathological tau–tau binding interaction which locks the repeat domains into a characteristic proteolytically stable configuration and one that is abnormally phase-shifted with respect to the tubulin-binding domains in this region of tau [25]. This templated prion-like interaction propagates and is amplified through repeated proteolytic digestion cycles [51] and can be modeled within the cell milieu [29]. Full-length and truncated tau bind to the core tau fragment with an estimated K_D of 20 nM, and binding is inhibited 10- to 50-fold by phosphorylation [30].

Recently, a cryo-electron microscopy structure of PHFs isolated from AD brain has been reported [31]. The core structure of these filaments consists of residues 306 to 378, and the structure can incorporate both three- and four-repeat tau isoforms. The structure is an in-register parallel β-sheet formed by a β-bend and β-helix motif, linked by β-strands [31].

In this study, we have used the truncated PHF-core tau fragment, based upon the core of the PHF [18,32] and which includes the PHF core region identified in the recently reported PHF structure [31]. The truncated fragment comprises 95 amino acids corresponding to residues 297–391 from the 441-residue tau isoform (4R2N). It is termed dGAE, where *d* identifies the N-terminal residue 297 and *GAE*, the three C-terminal residues terminating with Glu-391, as described in detail in Ref. [25]. dGAE was examined under non-reducing and reducing conditions. The 95-amino-acid peptide contains a single cysteine at position 322, and we have compared the assembly of wild-type dGAE with protein in which the Cys has been substituted with Ala (dGAE-C322A). The dGAE protein self-assembles into filaments that share the characteristics of amyloid (β-sheet content, cross-β X-ray fiber diffraction pattern) and that closely resemble the PHFs isolated from AD brains. We have investigated the contribution of disulfide formation of Cys322 and show that incubation in reducing conditions or introducing a C322A substitution leads to enhanced self-assembly and the production of long and highly ordered PHFs.

Results

Assembly of truncated tau protein

Recombinant truncated dGAE tau and dGAE-C322A were expressed in bacteria and purified by ion-exchange chromatography. Purified, soluble dGAE (100 μM) was incubated in phosphate buffer (PB), with and without 10 mM dithiothreitol (DTT). dGAE-C322A was prepared in the same manner (without DTT) and assembly into aggregates or filaments was monitored using thioflavin-S (ThS) fluorescence at intervals up to 48 h (Fig. 1). ThS has been previously shown to give an enhanced intensity when measuring tau assembly [33] and used to quantify PHFs [29]. ThS fluorescence intensity for reduced and non-reduced dGAE and dGAE-C322A increased with time indicating the gradual assembly into oligomers and filaments (Fig. 1a). ThS assays are very similar to thioflavin T (ThT) and will detect assembled structures above a certain threshold (depending on concentration). As has been shown frequently, ThT and ThS begin to show a signal at time points where small oligomeric structures can be observed by electron microscopy. The elongation of the fibrils correlates with an increase in fluorescence intensity. Indeed, we detect small oligomers by transmission electron microscopy (TEM) at the same time point as an increased ThS intensity. Each spectrum showed a similar lag-phase length; the final intensity of ThS fluorescence for dGAE-C322A after 48 h was slightly lower than for dGAE. This may reflect subtle changes in binding of ThS to the different species formed. Tyrosine fluorescence was monitored to follow changes in the environment of the tyrosine residue during assembly and, again, the data suggest similar assembly rates for non-reduced dGAE and dGAE-C322A. In the presence of DTT, the tyrosine fluorescence decreased more rapidly, consistent with an alternative assembly pathway. Circular dichroism (CD) spectra showed that the dGAE transitioned from a mainly random coil conformation, with a minimum at 198 nm, to one of

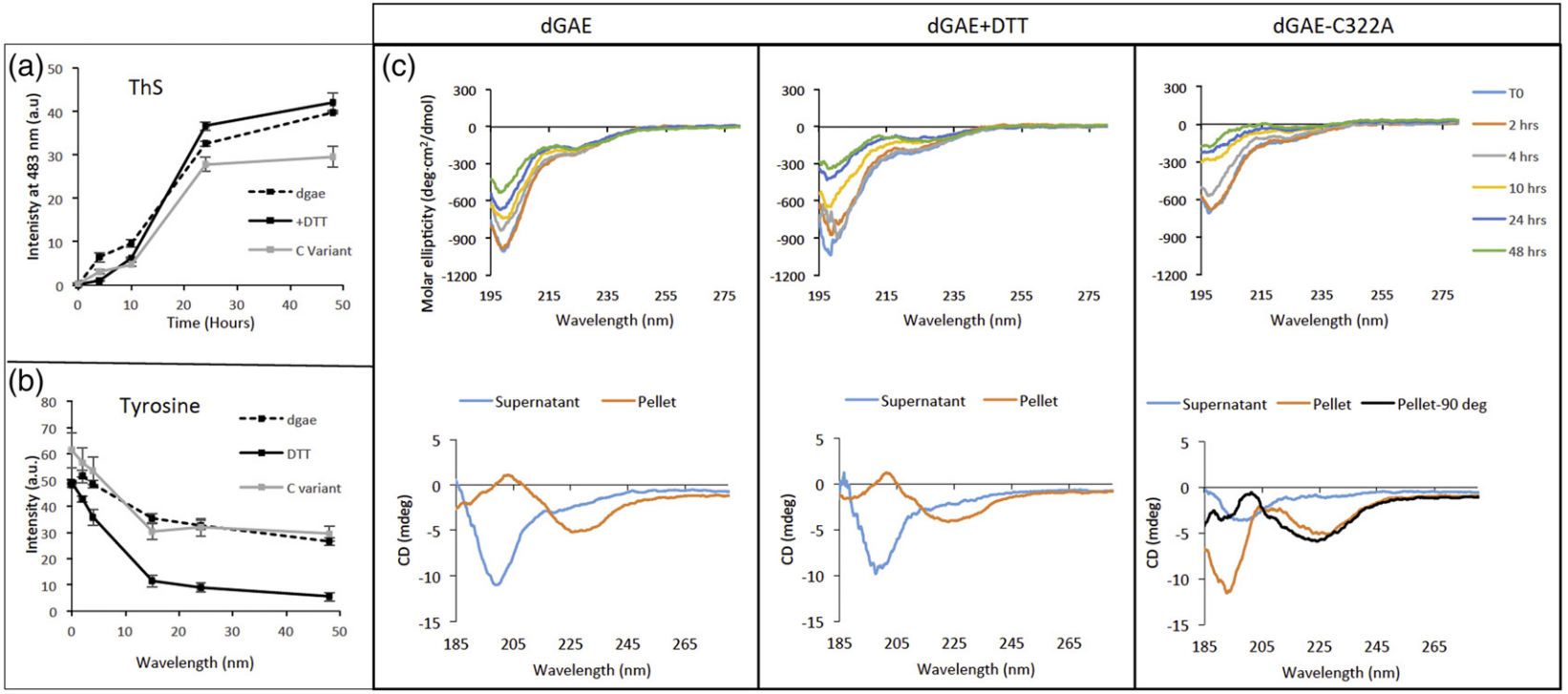

Fig. 1. Assembly of dGAE (100 μM) incubated in non-reducing and reducing conditions (with 10 mM DTT) and dGAE-C322A (100 μM) in PB (10 mM; pH 7.4). (a) ThS fluorescence assay showing assembly of all three samples over 48 h. (b) Fluorescence from tyrosine decreases over time during assembly suggesting a change in the environment of the tyrosine side-chain. Data expressed as mean ± S.E. (n = 3). (c) CD spectra of non-reducing and reducing dGAE and dGAE-C322A over time for the whole sample (top) and in the separated supernatant and pellet fractions (below). The whole samples show a reduction in intensity of the random coil signal (198 nm minimum) (see Fig. S1) and a relative increase in intensity at 218 nm with increased time. Following separation, random coil was observed in the supernatant and β-sheet in the pellet. For the separated samples, the y axis is given in millidegrees as the unknown concentrations did not allow for conversion to molar ellipticity.

increasing β-sheet conformation and reduced random coil (Fig. 1c). Random coil dominates the signal in the whole sample, so to investigate this further, samples were centrifuged at 20,000*g* to separate the supernatant and pellet and CD was performed on the separated samples (Fig. 1c). This revealed that the suspended pellet contains protein showing a strong red-shifted β-sheet signal with a minimum at 226 nm, while the supernatant contains protein that is predominantly random coil with a strong minimum at 197 nm. Under reducing conditions, dGAE gave a similar spectral profile to non-reduced dGAE. dGAE-C322A gave a very weak random coil signal in the supernatant fraction, suggesting a reduction in available soluble random coil protein. The spectrum from the dGAE-C322A pellet was unusual and contained minima at 194 nm and 230 nm. To ensure that this did not arise from alignment of fibrils giving rise to linear dichroism [34], the cuvette was rotated 90°. The spectra were very similar, suggesting that this spectral difference does arise from CD. A red-shifted signal to 230 nm for β-sheet has been observed previously for elongated amyloid fibrils made from α-synuclein and may arise from extended lengths of β-structure in long fibrils [35]. To compare the assembly of dGAE, dGAE with DTT and dGAE-C322A and to complement the results of ThS and tyrosine fluorescence, the intensity of the CD signal for the supernatant only, was plotted against time (Fig. S1). These results suggest that dGAE-C322A variant assembles more quickly than dGAE under reducing conditions and that both assemble more quickly than dGAE alone. Centrifugation of the samples results in difficulties in measuring protein concentrations in pellet and supernatant. Therefore, Advanced Protein Assay was used to compare the concentration of protein in the pellet and supernatant for dGAE and dGAE-C322A after incubation of 48 h (Fig. S2). The results confirmed that less dGAE C322A remains in the supernatant compared to dGAE, supporting the view that C322A assembles more effectively than dGAE.

TEM was performed to compare the morphology of the dGAE samples at time points from 0 to 48 h (Fig. 2). Assembly of dGAE was observed under non-reducing conditions showing the formation of small round particles, which developed into slightly elongated and laterally associated fibers after 10-h incubation and which did not elongate further by 48 h. In contrast, dGAE incubated with DTT under reducing conditions formed distinct fibrillar structures by 4 h, which continued to elongate up to 48 h. dGAE-C322A formed elongated structures by 4 h and numerous long fibrils by 24 h, which associated laterally by 48 h. The ThS fluorescence assay suggested that the assembly kinetics were similar for the three protein samples (Fig. 1a). However, TEM revealed significant differences in elongation and morphologies at the incubation time points examined (Fig. 2).

SDS-PAGE was conducted on samples treated in the same way as for fluorescence assays and TEM (Fig. 3). The whole sample was compared with separated supernatant and pellet fractions. dGAE ran as a doublet with mobilities of 10/12 kDa and a doublet with mobilities of 20/24 kDa (see Fig. 3a,

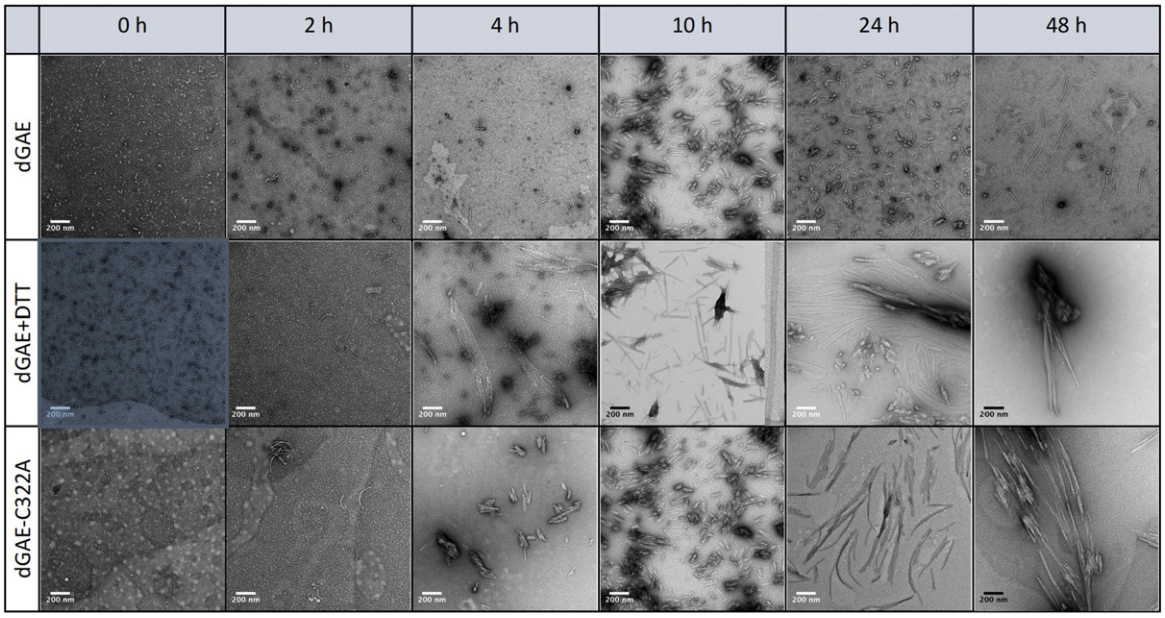

Fig. 2. TEM of dGAE (100 μM) incubated in non-reducing and reducing conditions (with 10 mM DTT) and dGAE-C322A (100 μM) in PB (10 mM; pH 7.4). dGAE assembles slowly to form small elongated fibers, while reduced dGAE forms fibrils by 10-h incubation. dGAE-C322A forms long fibrils that associate laterally by 48 h. The scale bars represent 200 nm.

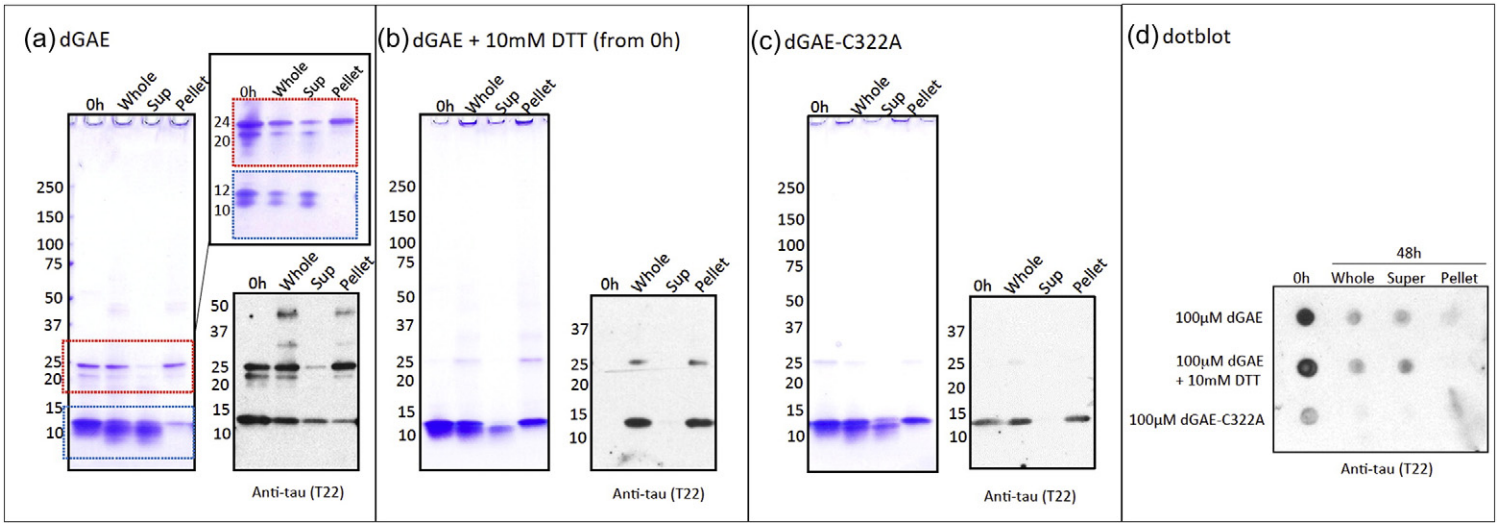

Fig. 3. SDS-PAGE and immunoblot of dGAE (100 μM) in (a) non-reducing and (b) reducing conditions (with 10 mM DTT) and (c) dGAE-C322A (100 μM). Each set of panels shows the results of Coomassie blue-stained SDS-PAGE gels (left) and immunoblot, using T22 anti-tau oligomer antibody (right), for the entire sample (whole) and the fractionated supernatant (sup) and pellet. Panel a shows an inset to highlight the positions of the doublet bands with reduced intensity. (d) Dot immunoblot for protein samples developed using T22 [36].

inset). Since the dGAE fragment has a theoretical molecular weight of 10.27 kDa, 10 kDa is likely to represent the monomer and 20 kDa, the corresponding dimer. The 12- and 24-kDa species are likely to represent alternative folding configurations of the dGAE monomer and dimer, respectively, having retarded gel mobility. After 48 h, the intensity of the bands in the whole sample was decreased and the bands in the supernatant appeared to be similar, but with markedly decreased dimer content. The pellet was enriched selectively for the 12- and 24-kDa species as well as for some weaker bands migrating at 37–50 kDa, suggesting the presence of higher-molecular-weight oligomers. The data suggest that the dGAE fragment is able to exist in two SDS-resistant conformations with different gel mobilities both as monomers and as dimers. The selective enrichment in the pellet of the 12- and 24-kDa species suggests that only one of the two conformations of dGAE is competent to aggregate into fibrils. To confirm that dGAE with DTT remained reduced following incubation for 48 h, free thiols were detected using Iodoacetimide-Oregon Green 488 (IAA-OG) assay (see Supplementary Information for methods). The results confirmed that the cysteine thiols remained free following incubation (Fig. S3). Immunoblotting was conducted using T22, an oligomer-specific antibody [36] to gain more information about the different mobility species. T22 bound selectively with the 12- and 24-kDa species in the pellet, but not with the more abundant 10-kDa monomer present in the supernatant. T22 also labeled higher-molecular-weight species at around 50 kDa in the pellet.

dGAE incubated under reducing conditions produced intense 10- and 12-kDa monomer bands at 0 and 48 h, but less of the corresponding dimers than seen in the absence of DTT. Coomassie blue staining also revealed non-migrating species of very-high-molecular-weight species in the wells. The monomer band remaining in the supernatant was substantially reduced and restricted to the species with 10-kDa mobility. The pellet contained both monomeric and dimeric species, corresponding exclusively to the 12- and 24-kDa variant. Comparison of these gels with those from non-reduced dGAE preparations suggests that the prevention of disulfide bond formation by the incubation with DTT facilitates the aggregation of the 12- and 24-kDa assembly-competent variants, leaving the 10-kDa monomer in the supernatant fraction. Also, incubation with DTT favors the formation of very-high-molecular-weight species which are either SDS insoluble or too large to enter the gel. Interestingly, immunoblotting again revealed preferential binding of T22 to the 12- and 24-kDa species, and not the 10- and 20-kDa variants seen by Coomassie staining in the whole preparation and in the supernatant fraction.

dGAE-C322A (Fig. 3) showed a predominant 12-kDa monomer and a less intense 10-kDa monomer at 0 h. After 48 h, the 12-kDa species was enriched in the pellet and the 10-kDa species enriched in the supernatant. Dimer formation was less than seen either for native dGAE fragment or following incubation in DTT, and again corresponded to the 24-kDa species. Immunoblotting showed that T22 reactivity was restricted to the 12-kDa species in the pellet with no binding to the 10-kDa species predominating in the supernatant fraction at 48 h. As a control, dGAE-C322A was also separated by SDS-PAGE in the presence of DTT and no change in the mobility was observed (data not shown).

In contrast to samples separated by SDS-PAGE, dot immunoblotting showed reactivity with T22 in all three samples at 0 h, and this is likely to correspond to the 12-kDa species. The intensity of T22 binding reduced after 48-h incubation in the whole and supernatant sample, and there was no binding of T22 to the pellet (Fig. 3b). This suggests that the 12-kDa band is in an oligomer-like conformation and that, following filament assembly, there is occlusion of the T22 epitope(s) leading to loss of T22 binding.

Collectively, the results of ThS, tyrosine fluorescence, TEM, and SDS-PAGE show that Cys-322 is unnecessary for filament assembly and that reduction of disulfide bonds, or substitution of Cys with Ala, promotes assembly to form longer and larger fibrillar structures, which sediment at low speed and that these are composed predominantly of the 12-kDa variant. Furthermore, the formation of a dimer in reducing conditions is suggestive of an alternative SDS-insoluble bond being formed in dGAE [37]. One possibility is the formation of dityrosine, which remains stable in reducing conditions [38].

X-ray fiber diffraction was performed for fibrils formed after 48-h incubation and revealed that all three proteins were able to form cross-β structures characteristic of amyloid fibrils (Fig. 4). The diffraction patterns shared a sharp, strong 4.7-Å and a 10-Å reflection, although the pattern from dGAE was poorly aligned due to the short fibrous structures formed. However, the diffraction pattern from dGAE-C322A showed a well-aligned fiber diffraction pattern with clear 4.7-Å reflection on the meridian and 9.5-Å reflection on the equator. A low-angle diffraction signal close to the backstop was also observed at approximately 28 Å, which may arise from ordered packing of the filaments (Fig. 4, inset). The patterns collected from the three fiber samples were very similar, and no obvious differences can be inferred from the patterns.

At 100 μM, dGAE forms only relatively short fibrillar structures even after incubation of up to 48 h. To investigate whether there is a concentration dependent effect leading to different fibril morphologies, dGAE was incubated at increasing concentrations from 100 μM to 400 μM.

CD was used to examine the secondary structures of the dGAE at different concentrations in the

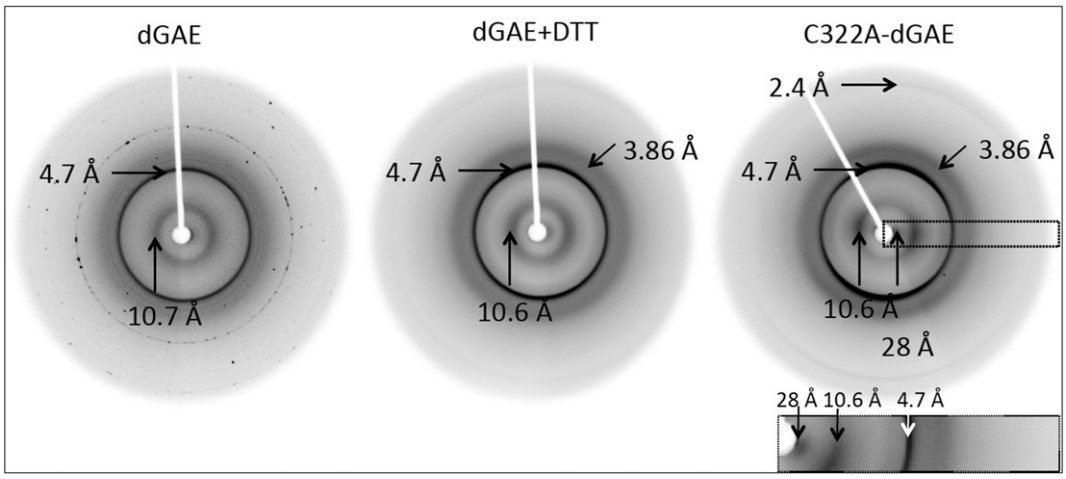

Fig. 4. X-ray fiber diffraction patterns from partially aligned fibrils. dGAE (100 μM) incubated in non-reducing and reducing conditions (with 10 mM DTT) and dGAE-C322A (100 μM) in PB (10 mM; pH 7.4) washed in milliQ water before alignment. The inset highlights the diffraction signals for dGAE-C322A to show the position of a 28-Å equatorial signal.

separated supernatant and pellet fractions. The CD spectra of the supernatant indicated the presence of random coil structure and signal intensities at 198 nm increased with concentration (Fig. S4), suggesting that a proportion of protein remains in solution. However, the CD spectra of dGAE pellet from different starting concentrations varied considerably. All spectra were consistent with a β-sheet conformation, but the positions of the minima differed slightly, probably reflecting differences in the supersecondary structural content of the filamentous structures in the pellet (Fig. 5a). ThS fluorescence was measured over 24 h and assembly rates for dGAE at low and high concentrations were compared. The findings suggest that the elongation rate increased with increased starting protein concentration (Fig. S5). TEM analysis showed changes in the lateral association and twisting of the filaments. Longer fibrils were observed at 250-μM concentration and at 300 μM, only long fibrils were observed while the smaller elongated particles were absent. At the highest concentration of dGAE tested (400 μM), highly ordered filaments with a clearly paired arrangement and a regular twist were observed (Fig. 5b). The mean (±SD) width was 16.18 ± 1.59 nm and 7.61 ± 1.24 nm with an approximate periodicity of 73.3 ± 4.37 nm (distributions shown in Fig. S6).

In order to investigate whether the molecular architecture of the filaments was dependent on concentration, X-ray fiber diffraction data were collected from all fiber samples prepared over a range of concentrations. Partially aligned fiber samples all exhibited characteristic cross-β diffraction signals (Fig. 5c, white and black arrows). The patterns were very similar to one another, with some small differences in alignment of the meridional and equatorial diffraction signals. TEM reveals differences in lateral packing and length but X-ray fiber diffraction reveals that the core structures were similar in all samples and consistent with the classical cross-β structure within the core of the protofilaments [39].

TEM and X-ray fiber diffraction were used to explore further whether there are any structural differences between dGAE incubated in non-reducing and reducing conditions at high concentrations (400 μM) (Fig. 6). TEM showed that dGAE under both conditions forms PHFs that have a helical periodicity of around 80 nm. This is similar to the helical periodicity observed for PHF isolated from AD tissue [18,32,40,41]. The truncated protein was able to form straight, paired filaments as well, although these were less common than the PHF morphology (approximately 10:90 ratio of SF to PHF) (see Fig. S7). SFs extracted from AD brain tissue constitute 5% of filaments [42]. X-ray fiber diffraction data showed the expected cross-β diffraction signals, but alignment was insufficient for further analysis. This is likely to be due to the very long filaments tangling and preventing good fiber orientation. However, the patterns show no evidence of any obvious differences between samples incubated with or without DTT.

Further analysis of the morphologies found in non-reduced and reduced dGAE samples is shown in Fig. 7. Non-reduced dGAE formed a majority of PHFs with a helical repeat of 73.3 ± 4.37 nm, while reduced dGAE formed PHFs with a helical repeat of 65.0 ± 6.9 nm and diameters of 17.8 ± 1.19 nm (wide) and 10.09 ± 2.42 nm (narrow). Occasionally, wider filaments were observed with a diameter of 20 nm, which appeared to be composed of more than one pair of filaments twisted together (Fig. 7). Fewer filaments with longer repeats of 83 nm were also observed. Overall, although the two samples contained a range of different species, there was

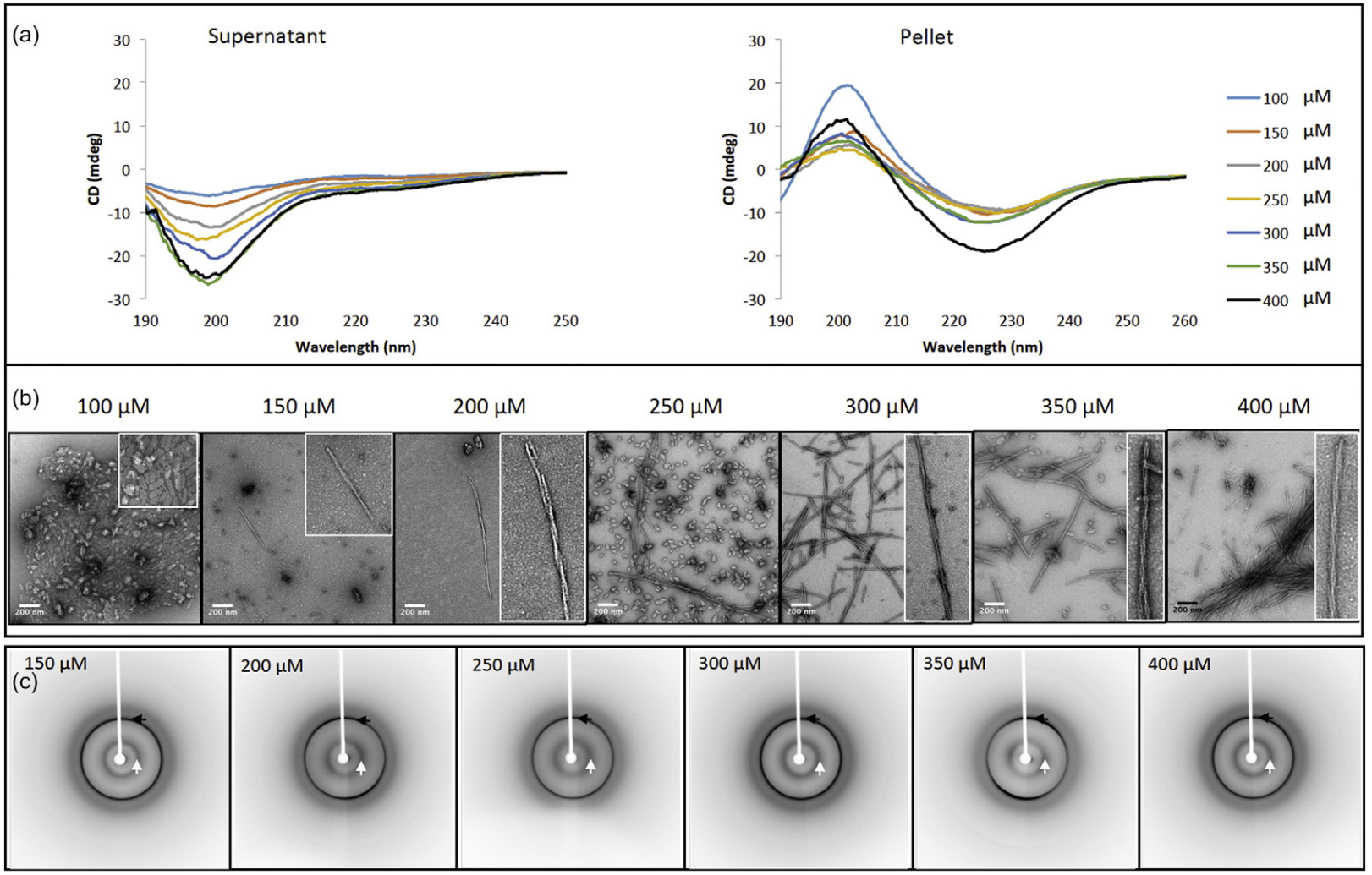

Fig. 5. Characterization of dGAE fibrils. Fibrils were formed using different starting concentrations of protein, as indicated, and incubated at 37 °C with agitation (700 rpm) for 48 h in PB (10 mM; pH 7.4). (a) Comparison between the CD spectra of supernatant and pellet fractions for each concentration of dGAE. The *y* axis is given in millidegrees as the concentrations did not allow for conversion to molar ellipticity. The intensity at 198 nm increased with increasing concentration (see Fig. S4). (b) dGAE fibril morphologies by TEM. The scale bars represent 200 nm (increased magnification panels included to highlight morphologies). (c) X-ray fiber diffraction patterns from partially aligned filament samples formed by dGAE, at the starting concentration indicated, showing the classic "cross-β" pattern (4.7 Å meridional is labeled with black arrow and 10–11 Å equatorial, with white arrow). Fiber axis is approximately vertical for all diffraction patterns.

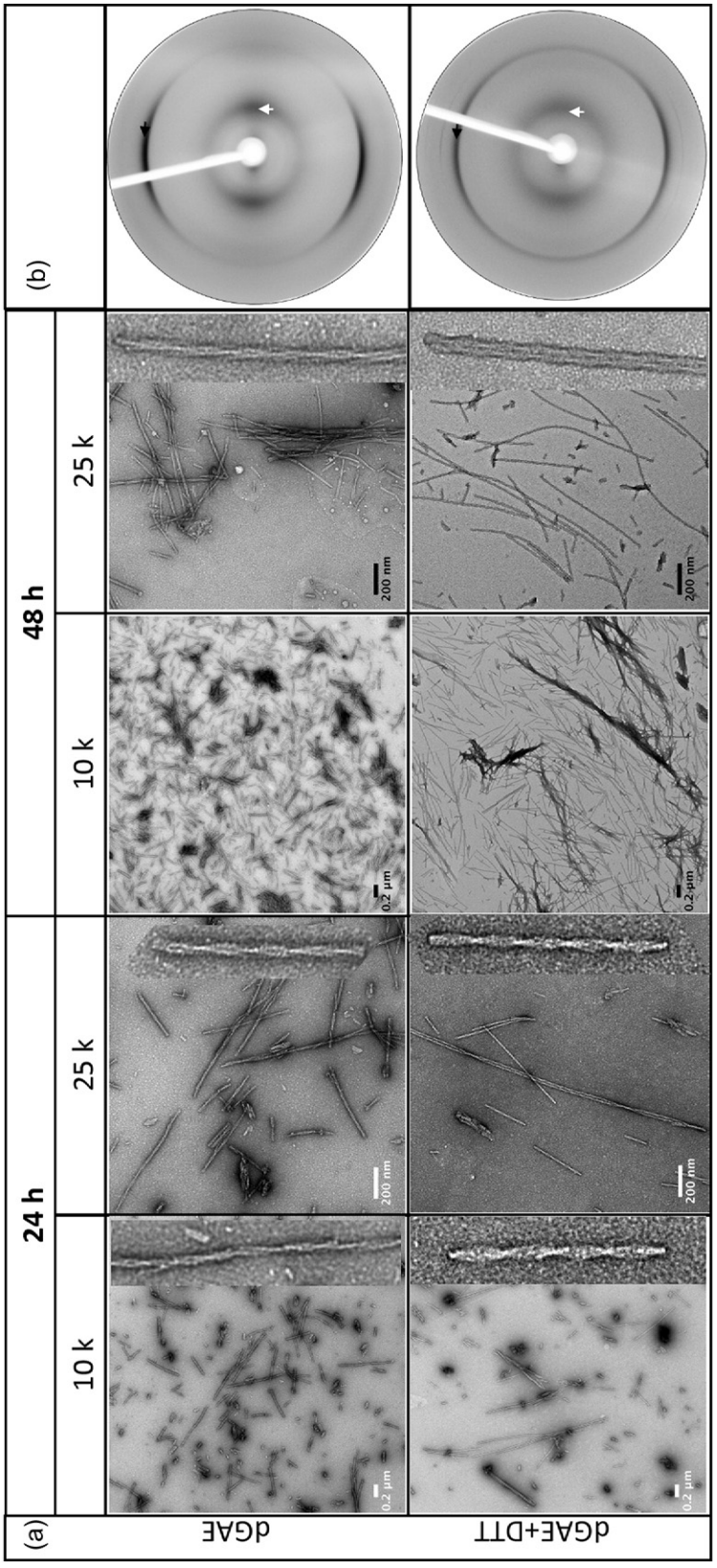

Fig. 6. TEM and X-ray fiber diffraction of non-reduced and reduced dGAE at 400 µM. (a) Electron micrographs showing the twisted features of the dGAE filaments after incubation for 24 and 48 h. The scale bars represent 200 nm, with selected insets showing 4× magnification. (b) Diffraction pattern obtained from dGAE (400 µM) without and with DTT.

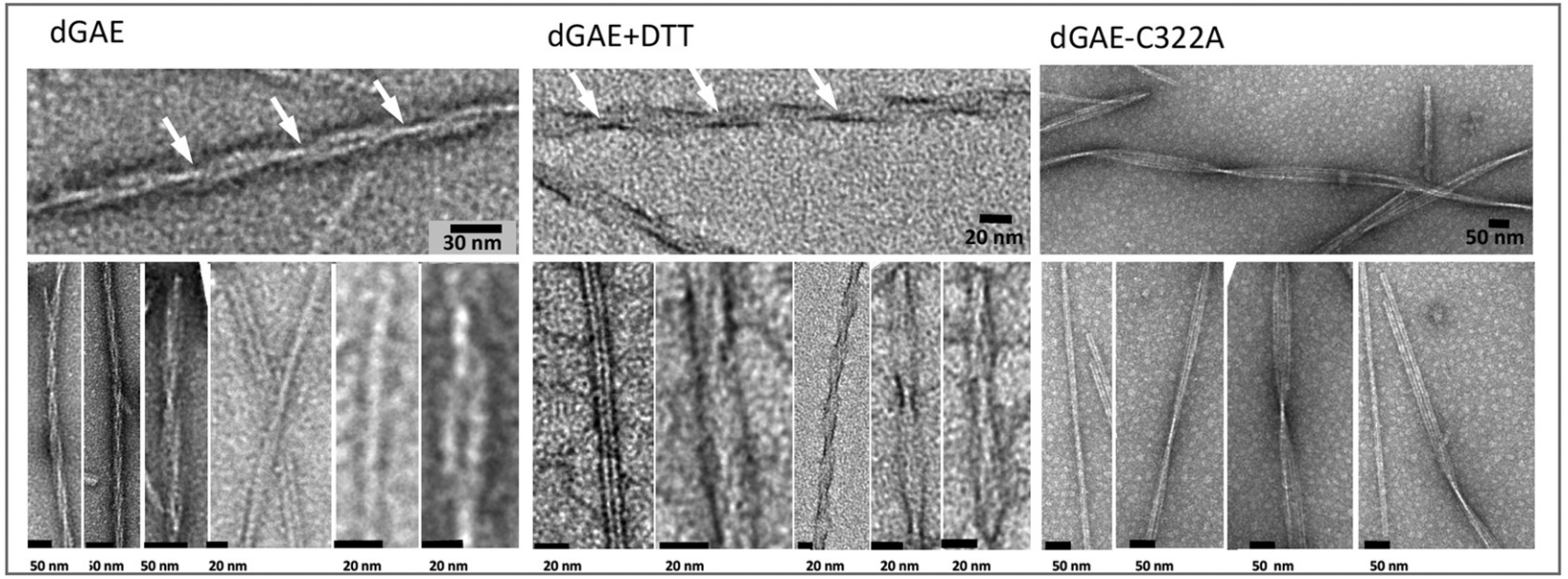

Fig. 7. Electron micrographs showing the detailed morphology of the dGAE assembled under non-reducing conditions, reducing conditions (400 μM) and dGAE-C322A (100 μM). Each condition yields PHFs and some SFs. There is very little difference between the morphology of dGAE assembled under non-reducing and reducing conditions, whereas dGAE-C322A formed twisted ribbons consisting of paired protofilaments. The scale bars are shown in nm.

no strong evidence to suggest that the structures were different when dGAE was incubated under non-reducing or reducing conditions. dGAE-C322A formed twisted ribbons consisting mostly of two protofilaments and with variable repeat lengths 392.5 ± 32.9 nm and occasionally, single protofilaments were observed (see Fig. 7).

Discussion

In this study, we have shown that a truncated form of tau corresponding to a 95-amino-acid region of the C-terminal domain (dGAE) is able to form filaments at physiological pH in the absence of any additives and that these closely resemble the PHFs found in neurofibrillary tangles in AD brain tissue. The dGAE fragment matches two of the species making up the structural core of the PHFs isolated from AD brain tissues [2]. Using a range of biophysical and structural approaches, we have shown that dGAE assembles in a concentration-dependent manner, with increasing β-sheet content and sharing the cross-β structure characteristic of all amyloid fibrils. Interestingly, small variations in the concentration of the protein lead to changes in the macromolecular appearance of the fibrils based upon electron microscopy observations and CD spectra. This highlights that very minor differences can have a large effect on the packing and overall morphology of filaments. Indeed, it has been shown that tau forms different filament morphologies when isolated from brain from different tauopathies, giving rise to different structural "strains" [40]. However, X-ray fiber diffraction indicated that the core cross-β structure was unaffected by these variations in macromolecular assembly.

We report that the assembly of the truncated core-tau fragment was enhanced by reducing conditions and the protein was able to form longer fibrils at the same concentration. To further explore the contribution of disulfide bond formation, we examined the assembly of dGAE-C322A and found that a species lacking any cysteine residues assembles rapidly and forms long, twisted filaments. The role for disulfide links in assembly has previously remained unclear as it has been impossible to study the effect of disulfide links on assembly in the absence of polyanionic additives, such as heparin, using full-length recombinant tau preparations [43]. We reveal that tau is able to form two types of dimer, one cysteine dependent and the other, cysteine independent. Full-length tau in COS cells has been previously shown to form cysteine-dependent and -independent dimers. Variants of full-length tau (C291A/C322A) that do not contain cysteines are able to form fibrils [43]. Furukawa *et al*. [44] argued that the morphologies of filaments assembled from full-length tau can be determined by disulfide status and thioflavine-T fluorescence and that disulfide-linked tau assembled more readily. However, electron microscopy showed that the filaments formed with disulfide bonds were shorter than those formed in the presence of DTT, similar to our findings. The K18 fragment (a different truncated four-repeat tau fragment; tau244–372) is able to form an intra-molecular disulfide-linked monomer which is not assembly-competent [45].

Our studies suggest that a truncated tau fragment corresponding to that found in the proteolytically stable core of the PHF exists in two alternative monomeric isoforms, one with a gel mobility of 10 kDa corresponding to the theoretical molecular weight of the fragment and a corresponding dimer of 20 kDa. The second has a gel mobility corresponding to 12 kDa and a corresponding dimer of 24 kDa. Exactly the same doublet was seen in the protein extracts from the PHF-core which first permitted the identification of a truncated tau protein fragment as a structural constituent of the PHFs formed in AD [2]. The formation of the 12-kDa variant does not depend on disulfide crosslinks, since it can form in the presence of an excess of DTT and also if there is a C322A substitution to produce a species lacking any cysteine residues.

The formation of the 20-kDa dimer was seen only in preparations favorable to disulfide bridge formation using native preparations of the dGAE fragment. Furthermore, the 10- and 20-kDa forms are enriched in the residual supernatant fraction left after filament assembly, whereas the 12- and 24-kDa forms are enriched selectively from the preparations of large aggregates isolated from slow-speed pellets. Conditions that inhibit filament assembly at low concentration (native dGAE at 100 μM), with formation of elongated spherical particles and short fibers at low concentration (100 μM), are also conditions favoring the formation of the 20-kDa dimer. The addition of a reducing agent (DTT) to the assembly solution results in the ability of the short, fibrillar dGAE structures to elongate to form long twisted fibrils. Furthermore, preventing the formation of disulfide bonds by replacing the only Cys residue in dGAE with Ala leads to the rapid formation of very long fibers. Increasing dGAE concentration leads to formation of long twisted fibrils, suggesting that at sufficiently high concentration species with disulfide crosslinks no longer affect the elongation step and that it is possible to overcome the inhibition associated with formation of disulfide dimers. We suggest that, at high concentration, the nucleation process is faster than when the protein contains disulfide bonds. Since there are no obvious differences in morphology or structure of the filaments forming from native dGAE at high concentration and those forming in conditions which prevent the formation of disulfide bonds, it is likely that there is a common assembly-competent precursor conformation and that the resulting PHFs do not contain any significant amounts of disulfide-linked

dGAE. We hypothesize that formation of assembly-incompetent dimers *via* disulfide linkages competes at the binding sites required for filament assembly, thereby limiting their extent. From this interpretation, conditions unfavorable to disulfide bridge formation would facilitate the formation of the assembly-competent variant and prevent other binding interactions with assembly-incompetent dimers which impede the formation of long PHF-like filaments (Fig. 8).

Our findings are consistent with the view that disulfide bond formation impedes PHF assembly. It has been shown that intramolecular disulfide bond formation stabilizes aggregation-prone tau peptides in conformations inconsistent with the formation of cross-β-structure [45]. Our findings are therefore at odds with the proposal that disulfide-linked dimer formation is a critical step in the pathological aggregation of tau protein in AD [44,46–48]. It is also at odds with the proposal that the tau aggregation inhibitor methylthioninium chloride (MTC) acts by preventing disulfide bridge formation [49,50]. Our data imply that if MTC were indeed able to impede cysteine crosslinking, it would have the effect of enhancing filament formation, which is not the case in cell-free or cell-based models or in disaggregation of PHFs isolated from AD brain tissue [29,51]. Further studies aiming to elucidate the correct mechanism of action of MTC are in progress.

Overall, our results show that the dGAE fragment is able to form two different species in solution under non-reducing conditions, an assembly-competent form and an assembly-incompetent form. It is striking that the 12/24-kDa variant is simultaneously enriched in the pellet and depleted from the supernatant after 48-h incubation in conditions that reduce disulfide bridge formation and also enhance the formation of long fibers, which closely resemble PHFs isolated from AD brain tissue [18,31,32]. It is also striking that it is the same variant that is preferentially recognized by the oligomer-specific antibody T22. Our results suggest, therefore, that there exists a specific conformation present in the 12-kDa variant, which makes it immunologically distinct from the alternative form which migrates at 10 kDa. Filaments assembled from the 12-kDa species have the same detailed morphological features as native PHFs isolated from AD brain tissue, including the characteristic longitudinal features in which four strands alternate with three strands in the twisted ribbon configuration, and showing only four strands in the flattened ribbon configuration. These features reflect the presence of the repeating C-shaped first identified in the native PHF core [18,32] and found also to be the repeating subunit of SFs [42]. It has been reported recently that the C-shaped subunit of the PHF core corresponds to a folded hairpin configuration of the core tau unit of the

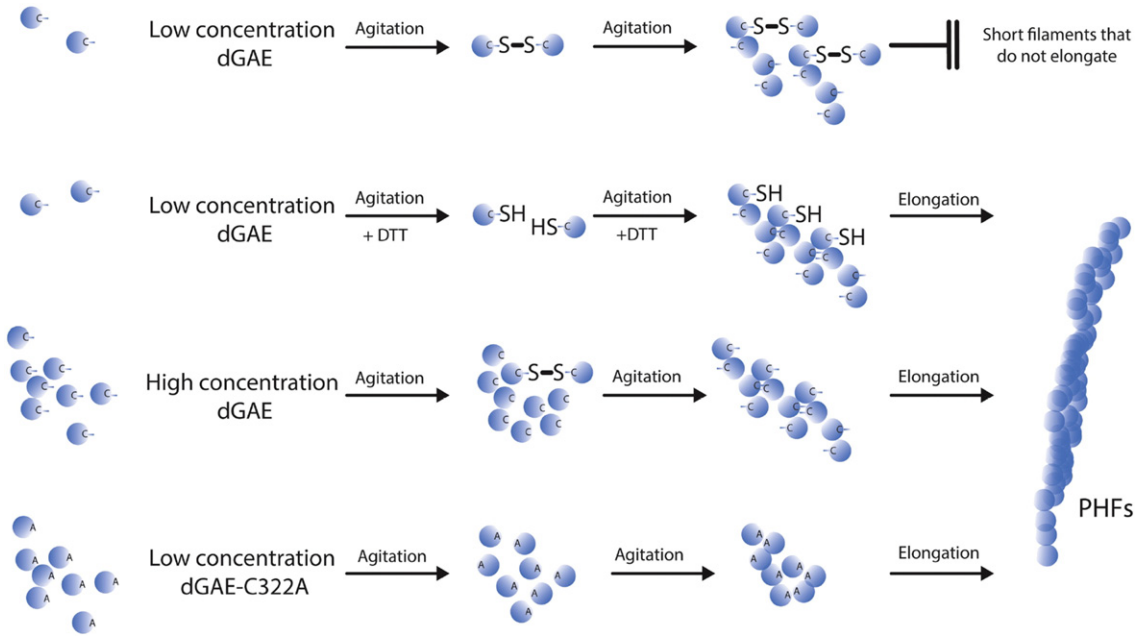

Fig. 8. Schematic showing the role for disulfide bonding in assembly. The initial dGAE solution contains monomers. At low concentration, the dGAE protein is able to form disulfide-linked dimers and with agitation, to elongate to form short filaments which cannot elongate further. This prevention of elongation can be overcome by the addition of DTT, which prevents formation of disulfide bonds and leads to the formation of an assembly competent intermediate that can elongate to form long PHFs. At high concentration of dGAE in non-reducing conditions, there is competition between formation of assembly competent and incompetent forms and long filaments can be formed. dGAE-C322A is unable to form disulfide bonds and is able to assemble rapidly to form long PHFs.

PHF matching closely the sequence of the dGAE fragment we have studied here [31]. In this structure, elucidated using cryo-electron microscopy analysis of *ex vivo* PHF and SF, the tau folds into a cross-β/β-helix structure in residues 306–378 [31] (Fig. S8). The structure also reveals that the position of the Cys side chain is buried between two sheets and would not be available for disulfide linking with Cys from another molecule (Fig. S8). This reinforces our findings that the disulfide-linked dimer is assembly incompetent. We therefore infer from the data we have presented that the property of assembly competence that we have associated with the 12-kDa variant is directly linked with the hairpin conformation of the repeat domain found in the PHF core and recognized selectively by T22.

Previous studies have shown that the tau unit corresponding to the dGAE fragment has the ability to bind full-length tau with high affinity and to template the reproduction of the core unit with loss of proteolytically susceptible domains outside the repeat domain in the presence of proteases [51]. The stable core of the PHF has a β-sheet structure [3], while the fuzzy coat is thought to be composed of unstructured protein chains [52] from the N- and C-terminal extensions of the molecule. Although there is considerable heterogeneity in the morphology of the filaments formed, which we have shown to depend on duration of incubation and concentration, the diffraction patterns of the different forms suggest a common underlying β-sheet molecular architecture.

We hypothesize on the basis of these results that underlying β-sheet architecture is inherent to and located within the conformation of the assembly-competent 12-kDa species. The property of dimerization shown on SDS-PAGE is not necessarily indicative of assembly competence and, indeed, it is likely that formation of the 20-kDa dimer is associated with inhibition of filament assembly. Our findings suggest that the therapeutic goal of optimizing inhibitors of tau aggregation may be served best by agents that either prevent the core tau protein fragment from adopting the assembly-competent configuration or block the association of assembly of 12-kDa subunits into toxic oligomers and filaments.

Materials and Methods

Assembly of truncated tau fibrils

Recombinant truncated tau297-391 (dGAE) and dGAE-C322A were expressed in bacteria and purified by P11 phosphocellulose chromatography as described previously [51,53], with minor modifications. In some cases, 2-(*N*-morpholino)ethanesulfonic acid (Mes), pH 6.25, was used instead of piperazine-*N*,*N*′-bis(ethanesulfonic acid) (Pipes) and the protein was heat treated [54] instead of using DE52 ion-exchange treatment prior to P11 chromatography. Protein fractions were eluted with buffer [50 mM Pipes (pH 6.8) or 50 mM Mes (pH 6.25), both supplemented with 1 mM EGTA, 5 mM EDTA, 0.2 mM $MgCl_2$, 5 mM 2-mercaptoethanol] containing 0.1–1 M KCl. The peak of protein elution was identified by protein assay (at 0.3–0.5 M KCl) and dialyzed against 80 mM Pipes buffer (pH 6.8), 1 mM EGTA, 5 mM EDTA, 0.2 mM $MgCl_2$, 5 mM 2-mercaptoethanol, or PB (10 mM; pH 7.4). Protein concentration, measured using Advanced Protein Assay Reagent (Cytoskeleton, Inc.) with bovine serum albumin as a standard, was in the range 2.7–4.9 mg/ml. The protein was diluted to 10 mM phosphate buffer (pH 7.4) at a range of concentrations (100–400 μM) for further analysis.

Investigating the role of disulfide bond on dGAE assembly

dGAE (100 μM) with and without DTT (10 mM) was incubated at 37 °C with agitation at 700 oscillations per minute (Eppendorf thermomixer C, Epppendorf, Germany) for 48 h. dGAE-C322A (100 μM) was incubated using the same assembly conditions. The assembly process was monitored using ThS fluorescence spectroscopy, tyrosine fluorescence spectroscopy, CD spectrometry, negative stain TEM, X-ray fiber diffraction, SDS-PAGE, and immunolabeling dot blot.

TEM

Electron microscopy grids were prepared by placing 4 μl of sample onto formvar/carbon-coated 400-mesh copper grids (Agar Scientific), blotting excess and then washing with 4 μl of 0.22 μM filtered milliQ water. Uranyl acetate (4 μl of 2% w/v) was placed on the grid for 1 min and then blotted, and the grid was allowed to air-dry. Electron micrograph images were collected using a JEOL JEM1400-Plus Transmission Electron Microscope operated at 120 kV. Camera is 4kx4K One View (Gatan), acquisitions were performed at 25 fps and automatically corrected for drift using Digital Micrograph (GMS3, Gatan).

CD

CD was performed using a Jasco Spectrometer J715 and spectra collected in triplicate at a maintained temperature of 21 °C. Protein samples (30 and 60 μl) were placed into 0.1- and 0.2-mm path length quartz cuvettes (Hellma), respectively, and scanned from 180 to 300 nm. Since the CD spectra were dominated by a random coil signal, samples were centrifuged at 20,000*g* for 30 min to separate fibrillar structures from the mixture. CD was then determined on the supernatant and pellet fractions

(40 µl) separately. CD data were converted into molar ellipticity (deg·cm^2·dmol^{-1}) where concentrations were known.

Tyrosine fluorescence

Spectra were collected for dGAE, dGAE with 10 mM DTT, and dGAE-C322A (140 µl, 100 µM) in a 10-mm cuvette. The excitation wavelength was 280 nm, and an emission scan between wavelength 290–500 nm was collected using a Varian Cary Eclipse Fluorescence Spectrophotometer. The sample compartment was set to 21 °C with a scan rate of 600 nm/min. The data represent three independent experiments.

ThS fluorescence

dGAE (20 µl) was mixed with ThS (280 µl, 5 µM) in 3-(*N*-morpholino)propanesulfonic acid (Mops) (20 mM, pH 6.8) and then added to a 10-mm path length cuvette. An emission scan between 450 and 600 nm was obtained. The compartment was set to 21 °C with a scan rate of 600 nm/min. The average of three spectra is used for each graph.

SDS-PAGE and immunoblotting

dGAE (100 µM; with or without 10 mM DTT) and dGAE-C322A were agitated at 700 rpm, 37 °C, for 48 h. Aliquots of the whole assembly mixture were taken at 0 and 48 h. After 48-h agitation, the whole assembly mixture was centrifuged at 20,000*g* for 30 min at 4 °C. The resulting supernatant was separated from the pellet, and the pellet was suspended in an equal volume of PB (10 mM; pH 7.4). The entire assembly mixture and the supernatant and pellet fractions were used for SDS-PAGE and immunoblotting (3 µl of each per lane). For SDS-PAGE, samples were mixed with SDS sample buffer (without reducing agent) and separated using a 4%–20% gradient Mini-Protean® TGX Precast gels (Bio-Rad) at 120 V, until the sample buffer reached the end of the gel. The gel was stained using Imperial Protein Stain (Thermo Scientific), following the manufacturer's instructions, before sealing the gel and scanning on a Canon ImageRunner Advance 6055i scanner.

For immunoblotting, the separated proteins on the gel were transferred onto Amersham™ Protran™ NC nitrocellulose membrane (0.45 µm) at 200 mA for 90 min. The membranes were blocked in 5% milk in Tris-buffered saline-Tween 20 (TBS-T; 50 mM Tris, 150 mM NaCl, pH7.4, 0.1% Tween 20) for 1 h rocking at room temperature. The membrane was incubated with T22, an antibody that recognizes oligomeric tau (ABN454; Merck Millipore), in 5% milk in TBS-T (1:1000) overnight at 4 °C. The membrane was incubated in secondary HRP-conjugated goat anti-rabbit antibody in 5% dried milk in TBS-T (1:10,000) for 1 h at room temperature. The membrane was developed using Clarity™ ECL blotting substrate (Bio-Rad), following the manufacturer's instructions, and then exposed to X-ray film. The membrane was washed 5 × 10 min in TBS-T in between antibody incubations.

For the dot blot, 3 µl of the whole assembly mixture, the supernatant and pellets were blotted onto Amersham Protran NC nitrocellulose membrane (0.45 µm) and were left to air dry. The membrane was rinsed in TBS-T and then immediately blocked overnight at 4 °C in 5% milk in TBS-T. The membrane was incubated with T22 (1:1000) for 1 h at room temperature, followed by secondary HRP-conjugated goat anti-rabbit antibody (1:10,000) for 1 h at room temperature. Proteins on the membrane were detected using Clarity ECL blotting substrate (Bio-Rad), following the manufacturer's instructions, and then exposed to X-ray film. The membrane was washed 5 × 10 min in TBS-T between each antibody incubation.

X-ray fiber diffraction

Samples were prepared for X-ray fiber diffraction by incubating dGAE, dGAE with DTT, and dGAE-C322A (diluted in 10 mM PB, pH 7.4) for 48 h to allow for the formation of fibrils at 37 °C and with agitation (700 oscillations per min). The resulting fibrils were collected by centrifugation (20,000*g*) and washed twice with water to remove buffer salts, and 10 µl of the sample was placed between wax-tipped capillary tubes allowed to dry overnight or dried onto a Teflon slide as described previously [55]. The partially aligned samples were mounted on a goniometer head and a diffraction pattern was collected using a Rigaku rotating anode fitted with Saturn CCD detector, using an oscillation of 0.5°. Exposure times were 30 or 60 s, and the specimen to detector distance was 50 or 100 mm, respectively. Diffraction data were converted to TIFF format using Mosflm [56] and inspected using CLEARER [57]. Measurements of the diffraction signals were taken using the module within CLEARER, and these were then entered into the unit cell determination module, to explore possible indexing of the diffraction signals to a unit cell.

Acknowledgments

The authors would like to thank Dr. Pascale Schellenberger and Dr. Julian Thorpe for valuable help with TEM. TEM work was performed at the School of Life Sciences TEM imaging center at the University of Sussex, which is supported by the Wellcome Trust and RM Phillips.

L.C.S. is supported by Alzheimer's Society and Alzheimer's Research UK Southcoast Network.

Appendix A. Supplementary data

Supplementary data to this article can be found online at https://doi.org/10.1016/j.jmb.2017.09.007.

Received 10 June 2017;
Received in revised form 8 September 2017;
Accepted 8 September 2017
Available online 15 September 2017

Keywords:
Alzheimer's disease;
tau;
neurofibrillary tangles;
paired helical filaments;
disulfide

Abbreviations used:
PHFs, paired helical filaments; SFs, straight filaments; AD, Alzheimer's disease; dGAE, truncated tau297-391; PB, phosphate buffer; DTT, dithiothreitol; ThS, thioflavin-S; ThT, thioflavin-T; TEM, transmission electron microscopy; CD, circular dichroism; MTC, methylthioninium chloride; TBS-T, Tris-buffered saline-Tween 20.

References

[1] D.J. Selkoe, The molecular pathology of Alzheimer's disease, Neuron 6 (1991) 487–498.
[2] C.M. Wischik, M. Novak, H.C. Thøgersen, P.C. Edwards, M.J. Runswick, R. Jakes, et al., Isolation of a fragment of tau derived from the core of the paired helical filament of Alzheimer disease, Proc. Natl. Acad. Sci. U. S. A. 85 (1988) 4506–4510.
[3] J. Berriman, L.C. Serpell, K.A. Oberg, A.L. Fink, M. Goedert, R.A. Crowther, Tau filaments from human brain and from in vitro assembly of recombinant protein show cross-beta structure, Proc. Natl. Acad. Sci. U. S. A. 100 (2003) 9034–9038.
[4] D.A. Kirschner, H. Inouye, L.K. Duffy, A. Sinclair, M. LInd, D.J. Selkoe, Synthetic peptide homologous to β-protein from Alzheimer's disease forms amyloid-like fibrils *in vitro*, Proc. Natl. Acad. Sci. U. S. A. 84 (1987) 6953–6957.
[5] D.W. Sanders, S.K. Kaufman, S.L. DeVos, A.M. Sharma, H. Mirbaha, A. Li, et al., Distinct tau prion strains propagate in cells and mice and define different tauopathies, Neuron 82 (2014) 1271–1288.
[6] F. Clavaguera, T. Bolmont, R.A. Crowther, D. Abramowski, S. Frank, A. Probst, et al., Transmission and spreading of tauopathy in transgenic mouse brain, Nat. Cell Biol. 11 (2009) 909–913.
[7] P.V. Arriagada, J.H. Growdon, E.T. Hedley-Whyte, B.T. Hyman, Neurofibrillary tangles but not senile plaques parallel duration and severity of Alzheimer's disease, Neurology 42 (1992) 631–639.
[8] G.K. Wilcock, M.M. Esiri, Plaques, tangles and dementia. A quantitative study, J. Neurol. Sci. 56 (1982) 343–356.
[9] E.B. Mukaetova-Ladinska, F. Garcia-Siera, J. Hurt, H.J. Gertz, J.H. Xuereb, R. Hills, et al., Staging of cytoskeletal and β-amyloid changes in human isocortex reveals biphasic synaptic protein response during progression of Alzheimer's disease, Am. J. Pathol. 157 (2000) 623–636.
[10] M. Maruyama, H. Shimada, T. Suhara, H. Shinotoh, B. Ji, J. Maeda, et al., Imaging of tau pathology in a tauopathy mouse model and in Alzheimer patients compared to normal controls, Neuron 79 (2013) 1094–1108.
[11] M.R. Brier, B. Gordon, K. Friedrichsen, J. McCarthy, A. Stern, J. Christensen, et al., Tau and Abeta imaging, CSF measures, and cognition in Alzheimer's disease, Sci. Transl. Med 8 (2016), 338ra66.
[12] S.N. Gomperts, J.J. Locascio, S.J. Makaretz, A. Schultz, C. Caso, N. Vasdev, et al., Tau positron emission tomographic imaging in the Lewy body diseases, JAMA Neurol. 73 (2016) 1334–1341.
[13] R. Smith, A. Puschmann, M. Scholl, T. Ohlsson, J. van Swieten, M. Honer, et al., 18F-AV-1451 tau PET imaging correlates strongly with tau neuropathology in MAPT mutation carriers, Brain 139 (2016) 2372–2379.
[14] T. Crowther, M. Goedert, C.M. Wischik, The repeat region of microtubule-associated protein tau forms part of the core of the paired helical filament of Alzheimer's disease, Ann. Med. 21 (1989) 127–132.
[15] L. Buée, T. Bussière, V. Buée-Scherrer, A. Delacourte, P.R. Hof, Tau protein isoforms, phosphorylation and role in neurodegenerative disorders, Brain Res. Rev. 33 (2000) 95–130.
[16] M. Bukar Maina, Y.K. Al-Hilaly, L.C. Serpell, Nuclear tau and its potential role in Alzheimer's disease, Biomolecules 6 (2016) 9.
[17] Z. Mansuroglu, H. Benhelli-Mokrani, V. Marcato, A. Sultan, M. Violet, A. Chauderlier, et al., Loss of tau protein affects the structure, transcription and repair of neuronal pericentromeric heterochromatin, Sci. Rep. 6 (2016) 33047.
[18] C.M. Wischik, R.A. Crowther, M. Stewart, M. Roth, Subunit structure of paired helical filaments in Alzheimer's disease, J. Cell Biol. 100 (1985) 1905–1912.
[19] R. Crowther, Tau protein and paired helical filaments of Alzheimer's disease, Curr. Opin. Struct. Biol. 3 (1993) 202–206.
[20] O. Schweers, E. Schönbrunn-Hanebeck, A. Marx, E. Mandelkow, Structural studies of tau protein and Alzheimer paired-helical filaments show no evidence for β-structure, J. Biol. Chem. 269 (1994) 24290–24297.
[21] M. Goedert, R. Jakes, M.G. Spillantini, M. Hasegawa, M.J. Smith, R.A. Crowther, Assembly of microtubule-associated protein tau into Alzheimer-like filaments induced by sulphated glycosaminoglycans, Nature 383 (1996) 550–553.
[22] M. Pérez, M. Arrasate, E. Montejo De Garcini, V. Munoz, J. Avila, In vitro assembly of tau protein: mapping the regions involved in filament formation, Biochemistry 40 (2001) 5983–5991.
[23] T. Kampers, M. Pangalos, H. Geerts, H. Wiech, E. Mandelkow, Assembly of paired helical filaments from mouse tau: implications for the neurofibrillary pathology in transgenic mouse models for Alzheimer's disease, FEBS Lett. 451 (1999) 39–44.
[24] R. Jakes, M. Novak, M. Davison, C.M. Wischik, Identification of 3- and 4-repeat tau isoforms within the PHF in Alzheimer's disease, EMBO J. 10 (1991) 2725–2729.
[25] M. Novak, J. Kabat, C.M. Wischik, Molecular characterization of the minimal protease resistant tau unit of the Alzheimer's disease paired helical filament, EMBO J. 12 (1993) 365–370.
[26] C.R. Harrington, E.B. Mukaetova-Ladinska, R. Hills, P.C. Edwards, E. Montejo de Garcini, M. Novak, et al., Measurement of distinct immunochemical presentations of tau protein in Alzheimer disease, Proc. Natl. Acad. Sci. U. S. A. 88 (1991) 5842–5846.

[27] R. Mena, P. Edwards, O. Perez-Olvera, C.M. Wischik, Monitoring pathological assembly of tau and beta-amyloid proteins in Alzheimer's disease, Acta Neuropathol. 89 (1995) 50–56.
[28] R. Skrabana, P. Kontsek, A. Mederlyova, K. Iqbal, M. Novak, Folding of Alzheimer's core PHF subunit revealed by monoclonal antibody 423, FEBS Lett. 568 (2004) 178–182.
[29] C.R. Harrington, J.M.D. Storey, S. Clunas, K.A. Harrington, D. Horsley, A. Ishaq, et al., Cellular models of aggregation-dependent template-directed proteolysis to characterize tau aggregation inhibitors for treatment of Alzheimer disease, J. Biol. Chem. 290 (2015) 10862–10875.
[30] R.Y. Lai, C.R. Harrington, C.M. Wischik, Absence of a role for phosphorylation in the tau pathology of Alzheimer's disease, Biomolecules. 6 (2016) 19.
[31] A.W.P. Fitzpatrick, B. Falcon, S. He, A.G. Murzin, G. Murshudov, H.J. Garringer, et al., Cryo-EM structures of tau filaments from Alzheimer's disease, Nature 547 (2017) 185–190.
[32] R.A. Crowther, C.M. Wischik, Image reconstruction of the Alzheimer paired helical filament, EMBO J. 4 (1985) 3661–3665.
[33] S. Barghorn, P. Davies, E. Mandelkow, Tau paired helical filaments from Alzheimer's disease brain and assembled in vitro are based on beta-structure in the core domain, Biochemistry 43 (2004) 1694–1703.
[34] K.L. Morris, A. Rodger, M.R. Hicks, M. Debulpaep, J. Schymkowitz, F. Rousseau, et al., Exploring the sequence-structure relationship for amyloid peptides, Biochem. J. 450 (2013) 275–283.
[35] L.C. Serpell, J. Berriman, R. Jakes, M. Goedert, R.A. Crowther, Fiber diffraction of synthetic α-synuclein filaments shows amyloid-like cross-β conformation, Proc. Natl. Acad. Sci. U. S. A. 97 (2000) 4897–4902.
[36] C.A. Lasagna-Reeves, D.L. Castillo-Carranza, U. Sengupta, J. Sarmiento, J. Troncoso, G.R. Jackson, et al., Identification of oligomers at early stages of tau aggregation in Alzheimer's disease, FASEB J. 26 (2012) 1946–1959.
[37] M.R. Reynolds, R.W. Berry, L.I. Binder, Site-specific nitration and oxidative dityrosine bridging of the tau protein by peroxynitrite: implications for Alzheimer's disease, Biochemistry 44 (2005) 1690–1700.
[38] Y.K. Al-Hilaly, L. Biasetti, B.J. Blakeman, S.J. Pollack, S. Zibaee, A. Abdul-Sada, et al., The involvement of dityrosine crosslinking in alpha-synuclein assembly and deposition in Lewy bodies in Parkinson's disease, Sci Rep 6 (2016) 39171.
[39] M. Sunde, L.C. Serpell, M. Bartlam, P.E. Fraser, M.B. Pepys, C.C. Blake, Common core structure of amyloid fibrils by synchrotron X-ray diffraction, J. Mol. Biol. 273 (1997) 729–739.
[40] M.G. Spillantini, R.A. Crowther, M. Goedert, Comparison of the neurofibrillary pathology in Alzheimer's disease and familial presenile dementia with tangles, Acta Neuropathol. 92 (1996) 42–48.
[41] H. Wille, G. Drewes, J. Biernat, E.M. Mandelkow, E. Mandelkow, Alzheimer-like paired helical filaments and anti-parallel dimers formed from microtubule-associated protein tau in vitro, J. Cell Biol. 118 (1992) 573–584.
[42] R. Crowther, Structural aspects of pathology in Alzheimer's disease, Biochim. Biophys. Acta 1096 (1991) 1–9.
[43] N. Sahara, S. Maeda, M. Murayama, T. Suzuki, N. Dohmae, S.H. Yen, et al., Assembly of two distinct dimers and higher-order oligomers from full-length tau, Eur. J. Neurosci. 25 (2007) 3020–3029.
[44] Y. Furukawa, K. Kaneko, N. Nukina, Tau protein assembles into isoform- and disulfide-dependent polymorphic fibrils with distinct structural properties, J. Biol. Chem. 286 (2011) 27236–27246.
[45] S. Walker, O. Ullman, C.M. Stultz, Using intramolecular disulfide bonds in tau protein to deduce structural features of aggregation-resistant conformations, J. Biol. Chem. 287 (2012) 9591–9600.
[46] O. Schweers, E.M. Mandelkow, J. Biernat, E. Mandelkow, Oxidation of cysteine-322 in the repeat domain of microtubule-associated protein tau controls the in vitro assembly of paired helical filaments, Proc. Natl. Acad. Sci. U. S. A. 92 (1995) 8463–8467.
[47] S. Barghorn, E. Mandelkow, Toward a unified scheme for the aggregation of tau into Alzheimer paired helical filaments, Biochemistry 41 (2002) 14885–14896.
[48] D. Kim, S. Lim, M.M. Haque, N. Ryoo, H.S. Hong, H. Rhim, et al., Identification of disulfide cross-linked tau dimer responsible for tau propagation, Sci Rep 5 (2015) 15231.
[49] E. Akoury, M. Pickhardt, M. Gajda, J. Biernat, E. Mandelkow, M. Zweckstetter, Mechanistic basis of phenothiazine-driven inhibition of Tau aggregation, Angew. Chem. 52 (2013) 3511–3515.
[50] A. Crowe, M.J. James, V.M. Lee, A.B. Smith III, J.Q. Trojanowski, C. Ballatore, et al., Aminothienopyridazines and methylene blue affect tau fibrillization via cysteine oxidation, J. Biol. Chem. 288 (2013) 11024–11037.
[51] C.M. Wischik, P.C. Edwards, R.Y.K. Lai, M. Roth, C.R. Harrington, Selective inhibition of Alzheimer disease-like tau aggregation by phenothiazines, Proc. Natl. Acad. Sci. U. S. A. 93 (1996) 11213–11218.
[52] G.P. Gellermann, H. Byrnes, A. Striebinger, K. Ullrich, R. Mueller, H. Hillen, et al., Abeta-globulomers are formed independently of the fibril pathway, Neurobiol. Dis. 30 (2008) 212–220.
[53] R. Brandt, M. Kempf, G. Lee, Expression and purification of tau for in vitro studies, in: J. Avila, R. Brandt, K.S. Kosik (Eds.), Brain Microtubule Associated Proteins: Modifications in Disease, Harwood Academic Publishers, Amsterdam 1997, pp. 245–257.
[54] J.C. Vera, C.I. Rivas, R.B. Maccioni, Heat-stable microtubule protein MAP-1 binds to microtubules and induces microtubule assembly, FEBS Lett. 232 (1988) 159–162.
[55] K.L. Morris, L.C. Serpell, X-ray fibre diffraction studies of amyloid fibrils, Methods Mol. Biol. 849 (2012) 121–135.
[56] M.D. Winn, An overview of the CCP4 project in protein crystallography: an example of a collaborative project, J. Synchrotron Radiat. 10 (2003) 23–25.
[57] O.S. Makin, P. Sikorski, L.C. Serpell, CLEARER: a new tool for the analysis of X-ray fibre diffraction patterns and diffraction simulation from atomic structural models, Appl. Cryst. 40 (2007) 966–972.